Available online at www.sciencedirect.com
ScienceDirect
Comput. Methods Appl. Mech. Engrg. 373 (2021) 113489
Computer methods in applied mechanics and engineering
www.elsevier.com/locate/cma

Optimal Bayesian experimental design for electrical impedance tomography in medical imaging

Ahmad Karimi[a,*], Leila Taghizadeh[a], Clemens Heitzinger[a,b]

[a] *Institute of Analysis and Scientific Computing, TU Wien, Wiedner Hauptstraße 8–10, 1040 Vienna, Austria*
[b] *School of Mathematical and Statistical Sciences, Arizona State University, Tempe, AZ 85287, USA*

Received 13 May 2020; received in revised form 19 September 2020; accepted 5 October 2020
Available online xxxx

Abstract

Optimal design of electronic devices such as sensors is essential since it results in more accurate output at the shortest possible time. In this work, we develop optimal Bayesian inversion for electrical impedance tomography (EIT) technology in order to improve the quality of medical images generated by EIT and to put this promising imaging technology into practice. We optimize Bayesian experimental design by maximizing the expected information gain in the Bayesian inversion process in order to design optimal experiments and obtain the most informative data about the unknown parameters. We present optimal experimental designs including optimal frequency and optimal electrode configuration, all of which result in the most accurate estimation of the unknown quantities to date and high-resolution EIT medical images, which are crucial for diagnostic purposes. Numerical results show the efficiency of the proposed optimal Bayesian inversion method for the EIT inverse problem.

Keywords: Bayesian experimental design; Expected information gain; Stochastic optimization; Electrical impedance tomography; Medical imaging

1. Introduction

Bayesian analysis in inverse modeling aims to compute expectations of so-called quantities of interest (QoI), constrained by forward PDE models, using probabilistic methods under a prior probability on uncertain PDE inputs, and taking the availability of possibly massive, noisy and redundant data into account. Prominent examples are climate and weather forecasts, subsurface flow, nanotechnology, life sciences and biomedical data. Bayesian inference tools have been so far applied successfully to many inverse problems in various applications (see for example [1–3]).

Electrical impedance tomography (EIT) [4–8] is an imaging technology which reconstructs electrical properties of the interior of a body using surface electrode measurements. The electrical and physical properties of a human body produce great information about the body interior for the identification and characterization of inclusions, for instance cancerous tissues. This phenomenon is exploited in EIT, where the electrical properties such as conductivity information is used to build images of the interior. This technology has attracted lots of attention since it possesses

* Corresponding author.
E-mail addresses: ahmad.karimi@tuwien.ac.at (A. Karimi), leila.taghizadeh@tuwien.ac.at (L. Taghizadeh), clemens.heitzinger@tuwien.ac.at (C. Heitzinger).

https://doi.org/10.1016/j.cma.2020.113489
0045-7825/

lots of practical advantages such as non-invasive, safe, portable and comparatively low cost devices. EIT technology has been applied for imaging in various medical fields; lung imaging [9–12] for example for the detection of pulmonary edema, breast imaging for the detection of abnormalities [13,14] and brain imaging for the study of epilepsy, migraine, and strokes [15–17] as a fast neuroimaging tool. Despite all advances, this charming technology is not yet competitive with computed tomography (CT) and magnetic resonance tomography (MRI) and has not yet been adopted widely as a clinical imaging tool; EIT is an ill-posed and nonlinear inverse problem [18], which suffers from low spatial resolution [19,20] and a poor signal-to-noise ratio (SNR) [21] compared to conventional tomographic imaging techniques such as CT and MRI. Using more electrodes increases the spatial resolution, but housing many electrodes is not always possible in real-life scenarios. Furthermore, using a smaller FEM mesh size may improve the image quality, but results in higher computational time and cost.

Mathematical modeling and numerical simulations of the EIT problem including uncertainty quantification and efficiently solving the tomography inverse problem are essential for optimal and efficient design of EIT devices in imaging technology. In [22], we developed a new PDE model for EIT and proposed Bayesian inversion techniques for solving the EIT inverse problem. In this paper, we develop optimal Bayesian inversion for EIT in order to infer internal electrical properties such as the conductivity of the body as accurately as possible, which results in high-resolution and high-quality clinical images. We reach the goal by developing optimal reconstruction algorithms and providing an optimal experimental recipe for the EIT inverse problem.

To present our recipe, one of the main questions which arises is how much information we can extract through a Bayesian approach from given experimental data and how we can do so in an optimal manner. To answer this question, we aim to calculate the expected information gain in the Bayesian inversion process, which specifically is the expected logarithmic ratio between the posterior and prior distributions of the unknown quantities. Optimizing this ratio as the objective function leads us to design real-time experiments and to obtain the most informative data about the model parameters, which results in the most accurate identification/estimation of the unknown quantities.

Some important questions also arise in presenting this novel methodology for the EIT problem: Which frequency within the allowed interval from 1 kHz to 1 MHz will be the optimal one and more informative in our real-world EIT applications? How and where should the electrodes at the body surface be located to reach the target expected information gain? And how many samples or iterations would be sufficient in Bayesian inversion in EIT real-time measurements? To answer these questions, we will maximize the expected information gain over the EIT design space: the new inversion recipe includes the presentation of optimal measurement frequency and optimal electrode placement in the real-time measurements of EIT, which lead to estimate the parameter of interest in the model, i.e., the conductivity of leg muscle, more accurately.

One of the difficulties in evaluating the expected information gain is that it involves nested integrations over a possibly high dimensional domain, which is computationally expensive. The second challenge is the optimization problem over a design space. In this paper, we develop a double-loop Monte-Carlo (DLMC) method for the EIT problem to calculate the expected information gain as well as simultaneous perturbation stochastic approximation (SPSA) to obtain optimal designs for the EIT problem.

This paper is organized as follows: optimal Bayesian inversion via the calculation of expected information gain is presented in Section 2. The nonlinear forward PDE model was first proposed in our previous work [22], but for the sake of accessibility, we provide some details on the nonlinear forward model equation and Bayesian inversion for the EIT inverse problem in Section 3. One of the main challenges is the sensitivity of the conductivity on the boundary measurements, which results from the severely ill-posed and nonlinear EIT inverse problem. The main goal of this paper is to deal with this challenge by optimizing the EIT experimental designs. More precisely, we aim to determine the optimal frequency and optimal electrode configuration in EIT based on the statistical interpretation of the reconstruction problem. Section 4 is devoted to presenting the optimal Bayesian experimental design including optimal frequency and electrode placement for EIT measurements by illustrating the numerical simulation results of optimization of expected information gain. Finally the conclusions are drawn in Section 5.

2. Optimal Bayesian experimental design

In the context of Bayesian inversion theory [23–26], there are two approaches to optimization of Bayesian experimental design: optimizing posterior covariance functionals with respect to the design/hyper parameters [27], and optimizing the Bayesian expected information gain (EIG) [28–31].

The first approach is based on the notion of distinguishability of the measurements. In the distinguishability approach, the optimality criterion is defined by maximizing the difference between measurements corresponding to two different predetermined parameter distributions and minimizing the volume of the posterior density. The second approach to optimize Bayesian inversion is to maximize the information about model uncertainty. In this approach, the expected information gain is taken as the design criterion into account and the optimal experiments are found from a continuously parametrized design space by inferring the model parameters from noisy data/observations in a Bayesian setting. The latter is the approach we follow in this paper.

2.1. Design criterion

In 1956, Lindley [32] suggested for the first time the use of Shannon expected information gain [33], which is based on Bayes' Theorem and the Kullback–Leibler (KL) divergence [34,35] from the posterior to the prior probability density functions of the unknown parameters, which is a popular information-based utility function to measure the information gain of data for Bayesian inverse problems. In order to formulate the approach in a Bayesian setting, we assume that unknown parameters are random variables. Suppose $(\Omega, \mathbb{A}, \mathbb{P})$ is a probability space, where Ω is a sample space, $\mathbb{A}$ is σ-Algebra of all events, and $\mathbb{P}$ is a probability measure on $(\Omega, \mathbb{A})$. Let the vector of real-valued random variables $\mathbf{q} \in \mathcal{Q}$, $\mathbf{y} \in \mathcal{Y}$ and $\mathbf{d} \in \mathcal{D}$ denote respectively the uncertain parameters, data/observations, and the design variables. Based on this approach, the expected information gain is defined as

$$I(\mathbf{d}) \coloneqq \mathbb{E}[D_{KL}] = \int_{\mathcal{Y}} \int_{\mathcal{Q}} p(\mathbf{q}|\mathbf{y}, \mathbf{d}) \log\Big(\frac{p(\mathbf{q}|\mathbf{y}, \mathbf{d})}{p(\mathbf{q})}\Big) \mathrm{d}\mathbf{q}\, p(\mathbf{y}|\mathbf{d}) \mathrm{d}\mathbf{y} \tag{1}$$

to estimate the efficiency of the proposed experiment set-ups. In the above expression, p denotes the density with respect to the Lebesgue measure and the simplification $p(\mathbf{q}|\mathbf{d}) = p(\mathbf{q})$ occurs since prior knowledge on the parameters does not vary with the experimental design. Furthermore, D_{KL} is the Kullback–Leibler (KL) divergence, which is defined as

$$D_{\mathrm{KL}} \coloneqq \int_{\mathcal{Q}} p(\mathbf{q}|\mathbf{y}, \mathbf{d}) \log\Big(\frac{p(\mathbf{q}|\mathbf{y}, \mathbf{d})}{p(\mathbf{q})}\Big) \mathrm{d}\mathbf{q} \tag{2}$$

as a measure of the information gain from posterior to prior or the information lost when the prior probability density function (PDF) is used to approximate the posterior PDF. The goal of optimal Bayesian experimental design (OBED) is to maximize the expected information gain over the design space $\mathcal{D}$ to find the optimal experimental design parameter(s)

$$\mathbf{d}^* = \arg\max_{\mathbf{d} \in \mathcal{D}} I(\mathbf{d}) \tag{3}$$

by providing the most informative observations.

2.2. Quantification of the design criterion

As the expected information gain (1) has no closed form, it should be approximated numerically. The numerical evaluation of the design criterion is computationally expensive, since it involves calculation of nested integrals on one hand, and searching the whole design space to find the maxima on the other hand. This evaluation is even harder and in some cases infeasible when, for instance, a higher-dimensional parameter or design space or an expensive forward solver is involved. Here, we propose a numerical methodology for the evaluation of the expected information gain of the EIT model parameters, namely the double-loop Monte-Carlo approximation, which is computationally efficient and speeds up the EIT Bayesian experimental design calculations.

2.2.1. Double-loop Monte-Carlo approximation

In the context of partial differential equations (PDEs), Monte-Carlo methods have been proven to dramatically reduce the computational complexity of the integration in Eq. (1). We propose an optimal double-loop Monte-Carlo method to efficiently compute the EIG of the parameters of interest in the EIT inverse problem using a Kullback–Leibler divergence measure in simulation-based optimal Bayesian experimental design. As Eq. (1) has no closed form, we first rewrite it as

$$I(\mathbf{d}) \coloneqq \mathbb{E}[D_{\mathrm{KL}}] = \int_{\mathcal{Y}} \int_{\mathcal{Q}} \log\Big(\frac{p(\mathbf{y}|\mathbf{q}, \mathbf{d})}{p(\mathbf{y}|\mathbf{d})}\Big) p(\mathbf{y}|\mathbf{q}, \mathbf{d}) p(\mathbf{q}) \mathrm{d}\mathbf{q}\mathrm{d}\mathbf{y} \tag{4}$$

using Bayes' theorem, in order to approximate it numerically. The double-loop Monte-Carlo approximation of I is defined as

$$I(\mathbf{d}) \approx \frac{1}{N}\sum_{i=1}^{N}\log\Big(\frac{p(\mathbf{y}_i|\mathbf{q}_i,\mathbf{d})}{\frac{1}{M}\sum_{j=1}^{M}p(\mathbf{y}_i|\mathbf{q}_{i,j},\mathbf{d})}\Big), \tag{5}$$

where $\mathbf{q}_i$ are parameter samples drawn from the prior $p(\mathbf{q})$ and $\mathbf{y}_i$ are data samples drawn from the likelihood $p(\mathbf{y}|\mathbf{q}_i,\mathbf{d})$. Furthermore, N and M are the number of samples in the outer and inner Monte-Carlo estimates, respectively. Algorithm 1 summarizes the necessary steps for the calculation of EIG using the double-loop Monte-Carlo method.

Algorithm 1 Algorithm to evaluate the EIG using double-loop Monte-Carlo

1. Draw a large size parameter samples $(\mathbf{q}_1,\ldots,\mathbf{q}_{N_0})$ from the prior $p(\mathbf{q})$.
2. Generate an index set of size $N_1 \leq N_0$ of random samples of the integers 1 to N_0 to obtain samples for the outer loop $(\mathbf{q}_1,\ldots,\mathbf{q}_{N_1})$.
3. Draw a data samples $(\mathbf{y}_1,\ldots,\mathbf{y}_{N_1})$ from the likelihood $p(\mathbf{y}|\mathbf{q}_i,\mathbf{d})$.
4. Generate index sets of size $M_1 \leq N_0$ of random samples of the integers 1 to N_0 to obtain samples for the inner loop $(\mathbf{q}_{1,i},\ldots,\mathbf{q}_{N_1,i})$ for $i = 1,\ldots,M_1$.
5. Evaluate the double-loop Monte-Carlo estimator Eq. (5).

2.3. Stochastic optimization

As mentioned, an optimal experimental design aims to maximize the worth of information of an experiment for statistical inference. This optimal process is of importance, especially for experiments that are long or expensive to perform. Hence, in order to solve the optimization problem of Bayesian experimental design (3), iterative search strategies and in particular stochastic optimization methods [36–39] instead of deterministic ones for high-dimensional problems are proposed, since the objective function is noisy. Here, we develop the simultaneous perturbation stochastic approximation (SPSA) algorithm [40,41] for the stochastic optimization of the noisy EIG, which is approximated by the double-loop Monte-Carlo method.

SPSA is a gradient-based optimization algorithm in the stochastic setting, which is used when only measurements of the objective function are available but no gradient information. The SPSA algorithm can be written in the general recursive stochastic approximation (SA) form

$$\mathbf{d}_{k+1} = \mathbf{d}_k - a_k\mathbf{g}_k(\mathbf{d}_k), \tag{6}$$

where k is the iteration number and $\mathbf{g}_k(\mathbf{d}_k)$ is the simultaneous perturbation estimate of the gradient, which is approximated by finite differences using only two random perturbations, i.e.,

$$\mathbf{g}_k(\mathbf{d}_k) = \frac{y(\mathbf{d}_k + c_k\boldsymbol{\Delta}_k) - y(\mathbf{d}_k - c_k\boldsymbol{\Delta}_k)}{2c_k}[\Delta_{k1}^{-1}, \Delta_{k2}^{-1},\ldots,\Delta_{kp}^{-1}]^T, \tag{7}$$

where $\boldsymbol{\Delta}_k = [\Delta_{k1}, \Delta_{k2},\ldots,\Delta_{kp}]^T$ is the mean-zero p-dimensional random perturbation vector with i.i.d. entries drawing from a user-specified distribution satisfying certain conditions [36, Sections 7.3 and 7.4], and y is the objective function. Furthermore a_k is a non-negative scalar gain coefficient and c_k is a positive scalar, which are defined by

$$a_k = \frac{a}{(C+k+1)^{\alpha}} \quad \text{and} \quad c_k = \frac{c}{(k+1)^{\gamma}},$$

where a, C, α, c and γ are parameters of the algorithm and their values can be found in [40]. The advantage of this stochastic approximation method is that in order to approximate the gradient only two function evaluations per step are required, while in a full finite difference scheme $2p$ evaluations are needed.

3. Bayesian inversion for EIT

In EIT, the aim is to reconstruct the conductivity distribution inside an object using boundary measurements. Information gained from the reconstructed conductivity is useful in a number of medical and engineering applications including cancer detection, monitoring for internal bleeding and determining body composition. Owing to increases in computational resources and knowledge transfer in EIT imaging methods (e.g. the EIDORS project), the interest in use of EIT in medical applications has dramatically increased over the past 20 years. In this section, we briefly review the forward and inverse EIT problem using the nonlinear elliptic PDE model, namely the nonlinear Poisson–Boltzmann equation, which we presented in [22] to model electrodes in a bioimpedance tomography device.

3.1. The linear model

The EIT forward problem is to find the electrostatic potential in the physical domain and then to calculate the electrical current flowing through the electrodes. Ignoring magnetic effects and assuming no internal current source in EIT problems, the (complex-valued) linear model is the Poisson equation

$$\nabla \cdot (A \nabla u) = 0, \tag{8}$$

where

$$A(x, \omega) := \sigma(x, \omega) + i\omega\epsilon(x, \omega) \tag{9}$$

is the admittivity, and σ and ϵ are the electric conductivity and permittivity, respectively. Also, ω is the frequency of the electrical current. Since we restrict the present discussion to static fields, i.e., $\omega \to 0+$, the admittivity is real and coincides with the static conductivity, i.e., $A = \sigma(x)$, which we use here. Moreover, the impedivity $\rho = 1/A$ is just the resistivity of the body [25]. The linear model (8) is widely used for modeling EIT; the Electrical Impedance Tomography and Diffuse Optical Tomography Reconstruction Software EIDORS [42] is based on this model equation.

To find the boundary conditions, we assume that there are L contact electrodes e_ℓ, which are attached to the surface of the body, i.e., $e_\ell \subset \partial D$, $1 \leq \ell \leq L$, such that $\overline{e}_\ell \cap \overline{e}_k = \emptyset$ for $\ell \neq k$. We assume that the electrodes conduct perfectly, and thus the tangential electrical field vanishes along the electrodes. Then, possible boundary conditions on the electrodes are the Dirichlet boundary conditions

$$u(x) = U_\ell, \quad x \in e_\ell, \quad 1 \leq \ell \leq L. \tag{10}$$

We also assume that no current flows in and out of the body between the electrodes, which leads to the zero Neumann boundary conditions

$$\frac{\partial u(x)}{\partial \mathbf{n}} = 0, \quad x \in \partial D \backslash \bigcup_{\ell=1}^{L} e_\ell. \tag{11}$$

3.2. The nonlinear model

To extend the model, we consider free charges of the background medium in the equation. Assuming that the energies of all ions in the electric field are distributed according to a Boltzmann distribution, we define the charge density of free charges in the system by

$$f_{\text{free}} := \eta(\exp(-\beta u) - \exp(\beta u)) = -2\eta \sinh(\beta u),$$

where η is the ion accessibility function. The constant β is defined as $\beta := 1/U_T$, where U_T is the thermal voltage at room temperature and it is defined by $U_T := k_B T/q$ in terms of the Boltzmann constant k_B and the temperature T, and $q > 0$ the elementary charge. Here, we assume that the charge of single positive and negative charge carriers is the same. In the definition of charge density of free charges, the exponential terms stem from the Boltzmann distributions for two species of ions, which leads to sinh in the model.

Adding charge density of free charges f_{free} to the fixed charges f_{fixed} (for simplicity we denote it by f in the equation), we arrive at the nonlinear Poisson–Boltzmann equation

$$-\nabla \cdot (A(x) \nabla u(x)) = f(x) - 2\eta(x) \sinh(\beta u(x))$$

as the extended model for the EIT problem. Therefore, the new forward problem describing EIT is to find the potential u in the main object D, given the conductivity A, the voltage pattern $U = (U_1, \ldots, U_L)^T$, the ion accessibility function η, and the concentration f of fixed charges, that solves the (real-valued) nonlinear elliptic PDE

$$-\nabla \cdot (A(x)\nabla u(x)) + 2\eta(x)\sinh(\beta u(x)) = f(x) \qquad \forall x \in D, \tag{12a}$$

$$u(x) = U_\ell \qquad \forall x \in e_\ell, \tag{12b}$$

$$\frac{\partial u(x)}{\partial \mathbf{n}} = 0 \qquad \forall x \in \partial D \backslash \bigcup_{\ell=1}^{L} e_\ell. \tag{12c}$$

As mentioned before, in every measurement pattern a potential is applied to the electrodes and the resulting electrical current on the rest of the electrodes is measured. The electrical current flowing through the electrodes in the EIT problem [6] is calculated by

$$I_\ell = \int_{e_\ell} A \frac{\partial u(x)}{\partial \mathbf{n}} ds, \qquad 1 \le \ell \le L. \tag{13}$$

The nonlinear Poisson–Boltzmann equation (12) has a unique solution and a pointwise estimate for the solution of the equation has been presented in [43]. The required assumptions for the existence of a unique solution are listed below.

Assumptions 1. The conductivity $A\colon D \to \mathbb{R}^{2\times 2}$ and the voltage simulation pattern $\{U_\ell\}_{\ell=1}^{L} \in \mathbb{R}^L$ satisfy the following assumptions:

1. The coefficient $A\colon D \to \mathbb{R}^{2\times 2}$ is a piecewise constant-valued matrix, which is uniformly elliptic and satisfies

$$A \in L^\infty(D; \mathbb{R}^{2\times 2}), \quad \operatorname*{ess\,inf}_{x\in D} A(x) = A^- > 0 \tag{14}$$

   and contains the conductivity of the inclusion and the background medium, as the two materials are different in their physical properties.
2. The voltages applied to the electrodes are chosen such that $\sum_{\ell=1}^{L} U_\ell = 0$.

To solve the proposed EIT model, the first order Galerkin finite element method is used and in order to illustrate the numerical solution, a cross-section of a human right leg is assumed as the computational domain, where eight electrodes are attached to its boundary. Fig. 1 (right) shows the domain with a finite element discretization. In this figure (left), three different subdomains are displayed: the first subdomain is a circular bone (in dark blue) surrounded by the second subdomain, the muscle (in brown), which itself consists of many partitions, and the rest is fat (in blue). Each subdomain has its own electrical conductivity and in the solution of the forward problem the FEM mesh is aligned with the inclusions such that each element has a constant value for the coefficient A.

Assuming that voltages of ± 10 V are applied to the injection electrode pair under the neighboring/adjacent method, Fig. 2 displays the obtained electrical potential as the solution of the model equation on the simulation domain for three injection patterns.

3.3. The EIT inverse problem

The EIT inverse problem is to reconstruct the electrical and physical properties of the body interior, given the electrode measurements on its surface. To solve this inverse problem, we propose Bayesian inversion techniques, in which the solution of the inverse problem is the posterior density that best reflects the distribution of the parameters based on the observations [23]. As the observations or measurements are subject to noise and the observational noise, i.e., the error e due to modeling and measurement, is unbiased and i.i.d., it can be represented by random variables as

$$M = G(Q) + e, \tag{15}$$

where e is a mean-zero random variable, M a given random variable representing observed data or measurements with realizations $y = M(\omega)$ and Q an uncertain random variable with realizations $q = Q(\omega)$ representing parameters

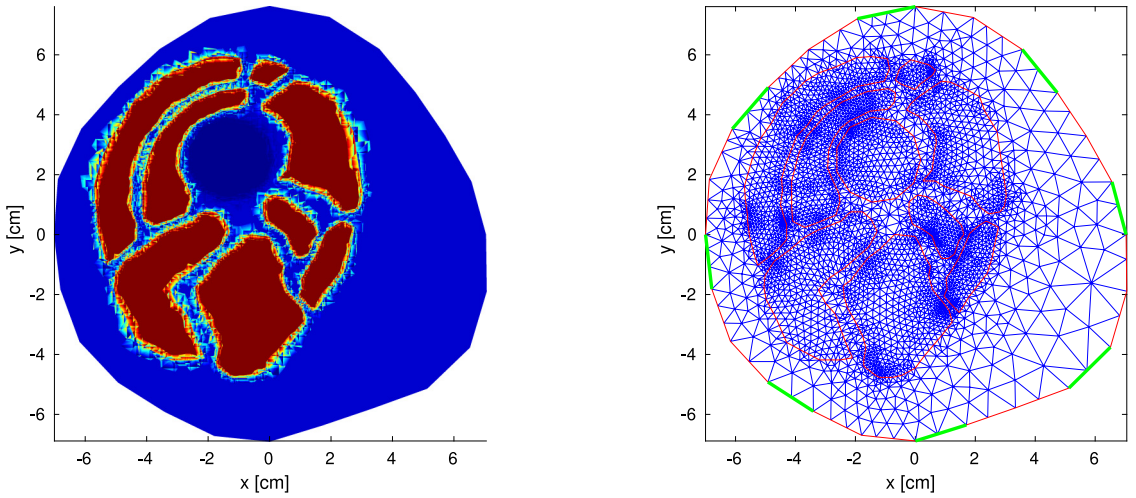

Fig. 1. EIT domain: cross-section of a right leg illustrating a schematic of the three subdomains (left) and the discretization by a FEM mesh (right) used for solving the forward problem. (For interpretation of the references to color in this figure legend, the reader is referred to the web version of this article.)

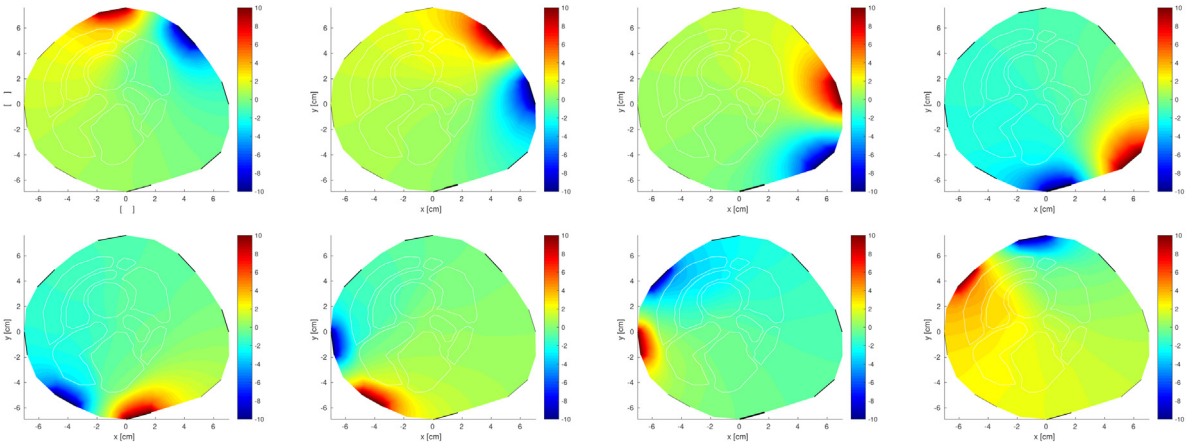

Fig. 2. Solution of the nonlinear forward problem (in Volt) using the neighboring injection method illustrated in 8 patterns in the frequency of 50 kHz for a cross-section of a right leg.

to be estimated. To describe the Bayesian inverse problem, we assume that for $O_i \in V^*, i = 1, 2, \ldots, m$, which denote m continuous, linear observation functionals on V, we define the forward mapping $G\colon X \to \mathbb{R}^m$ as

$$X \ni q \mapsto G(q) := \Big(O_1(u(\cdot, q)), \ldots, O_m(u(\cdot, q))\Big) \in \mathbb{R}^m,$$

which takes one realization of input Q to a noisy set of observations, where $u \in V$ is the solution of the forward PDE [44,45].

To describe the Bayesian approach on function spaces, we formulate Bayes' Theorem in a measure-theoretic framework, which is suitable for problems on infinite-dimensional spaces. To this end, assume that $(X, \|\cdot\|_X)$ (infinite-dimensional) and $(Y, \|\cdot\|_Y)$ (possibly infinite-dimensional) are separable Banach spaces and $q \in X$ is a random variable distributed according to measure μ_0 on X, in which our prior beliefs about the unknown parameter q are described. We assume the distribution of the measurement error e (data likelihood) is defined by

$$\pi(y|q) := \pi(y - G(q)) \tag{16}$$

to calculate the posterior probability measure μ^y for $q \in X$ given $y \in Y$, which leads to

$$\pi(q|y) = \frac{\pi_0(q)\pi(y - G(q))}{\int_{\mathbb{R}^p} \pi_0(q)\pi(y - G(q))\mathrm{d}q} \tag{17}$$

using Bayes' formula, where π_0 and π are the prior and posterior density functions and correspond to the probability measures μ_0 and μ^y, respectively. Thus, we have

$$\pi(q|y) \propto \pi_0(q)\pi(y - G(q)) \tag{18}$$

with a constant of proportionality depending only on y.

As in infinite-dimensional spaces there is no density with respect to the Lebesgue measure, Bayes' rule should be interpreted as providing the Radon–Nikodym derivative between the posterior measure $\mu^y(\mathrm{d}q) = P(\mathrm{d}q|y)$ (with density $\pi(q|y)$) and the prior measure $\mu_0(\mathrm{d}q) = P(\mathrm{d}q)$ (with density π_0), yielding

$$\frac{\mathrm{d}\mu^y}{\mathrm{d}\mu_0}(q) \propto \pi(y - G(q)). \tag{19}$$

Without loss of generality, we can view the right-hand side as the exponential of the negative of $\Phi(q, y)$, where $\Phi\colon X \times Y \to \mathbb{R}$ is called a potential. Hence, Eq. (19) can be rewritten as

$$\frac{\mathrm{d}\mu^y}{\mathrm{d}\mu_0}(q) \propto \exp(-\Phi(q, y)), \tag{20}$$

since the density π is nonnegative [46]. Furthermore, the posterior measure μ^y in some PDE inverse problems can be formulated as

$$\frac{\mathrm{d}\mu^y}{\mathrm{d}\mu_0}(q) = \frac{1}{C(y)} \exp(-\Phi(q, y)), \tag{21}$$

where $C(y)$ is a normalization constant and chosen such that μ^y is a probability measure, i.e.,

$$C(y) := \int_X \exp(-\Phi(q, y))\mathrm{d}\mu_0(q). \tag{22}$$

Furthermore, we assume that $\mu_0(X) = 1$ holds for the infinite-dimensional separable Banach space X.

The goal is to show that the posterior measure μ^y of the form (21) is well-defined and that the problem is well-posed with respect to its dependence on the data. To this end, the function $\Phi\colon X \times Y \to \mathbb{R}$ should have essential properties, namely lower and upper bounds and the Lipschitz property in q and y. As this function is defined in terms of the function $G\colon X \to \mathbb{R}^m$, it is sufficient to prove the following properties of the function G corresponding to the inverse problem of interest. This implies that $\Phi\colon X \times \mathbb{R}^m \to \mathbb{R}$ satisfies Assumption 2.6 in [46] with $(Y, \|\cdot\|_Y) = (\mathbb{R}^m, |\cdot|)$.

Assumptions 2. The function $G\colon X \to \mathbb{R}^m$ has the following properties.

1. For every $\varepsilon > 0$, there exists a $Z(\varepsilon) \in \mathbb{R}$ such that the inequality

$$|G(q)| \leq \exp(\varepsilon\|q\|_X^2 + Z(\varepsilon)) \tag{23}$$

holds for all $q \in X$.

2. For every $r > 0$, there exists a $K(r) > 0$ such that the inequality

$$|G(q_1) - G(q_2)| \leq K(r)\|q_1 - q_2\|_X \tag{24}$$

holds for all $q_1, q_2 \in X$ with $\max(\|q_1\|_X, \|q_2\|_X) < r$.

To prove the well-definedness of the posterior measure and well-posedness of the EIT Bayesian inversion, we need to verify if the bounds and Lipschitz properties in Assumption 2 hold true when G is given by the solution of the (real-valued) nonlinear elliptic PDE model (12) (assuming that $f = 0$ and g is the Dirichlet data). Theorem 1 presents boundedness and Lipschitz continuity of the solution of the nonlinear EIT model by functions of the parameters, which we need for the well-posedness of the Bayesian inversion for the new model. More details of the proof can be found in [22, Proposition 1].

Theorem 1. *Suppose the real-valued nonlinear elliptic equation (12) (assuming that $f = 0$ and g is the Dirichlet data) holds in the bounded domain $D \subset \mathbb{R}^n$, $n \in \{2, 3\}$, with a smooth boundary ∂D and $A := e^q =: \eta$, where $q \in L^\infty(D)$. Then, the estimate*

$$\|u\|_{H^1} \leq He^{2\|q\|_{L^\infty}} \tag{25}$$

holds for all $q \in L^\infty(D)$, and the estimate

$$\|u_1 - u_2\|_{H^1} \leq Se^{4\max(\|q_1\|_{L^\infty(D)}, \|q_2\|_{L^\infty(D)})}\|q_1 - q_2\|_{L^\infty(D)} \tag{26}$$

holds for all $q_1, q_2 \in L^\infty(D)$, where $H = H(\|\nabla \overline{g}\|_{L^2(D)})$ and $S = S(\|\nabla \overline{g}\|_{L^2(D)})$ are functions and $\overline{g} \in L^2(D)$ is the Dirichlet lift of g.

Proof. We substitute $v := u - \overline{g}$ in (12), where g is the Dirichlet data and $\overline{g}$ is the Dirichlet lift of g. In order to find estimates (25), we take the inner product with any $v \in H_0^1(D)$, which leads to

$$I := \left| \int A\nabla v \cdot \nabla v \right| = \left| -\int A\nabla \overline{g} \cdot \nabla v - \int 2\eta \sinh(\beta(\overline{g} + v))v \right|,$$

where $A = e^q$. Using $\eta = e^q$ and $\sinh(\beta(\overline{g} + v)) = (e^{\beta(\overline{g}+v)} - e^{-\beta(\overline{g}+v)})/2$ as well as the triangle inequality, we find

$$e^{-\|q\|_{L^\infty}}\|\nabla v\|_{L^2}^2 \leq I \leq \left| \int e^q \nabla \overline{g} \cdot \nabla v \right| + \left| \int e^q e^{\beta(\overline{g}+v)} v \right| + \left| \int e^q e^{-\beta(\overline{g}+v)} v \right|.$$

Using the Cauchy–Schwarz and Poincaré inequalities and $\kappa \leq u = \overline{g} + v \leq \lambda$, which is a pointwise estimate [43] for the solution of the Poisson–Boltzmann equation, we can write

$$\begin{aligned} \|\nabla u\|_{L^2} &\leq \|\nabla v\|_{L^2} + \|\nabla \overline{g}\|_{L^2} \\ &\leq 2C_p e^{2\|q\|_{L^\infty}}(\|\nabla \overline{g}\|_{L^2} + e^{|\beta\lambda|} + e^{|\beta\kappa|}) \\ &= H_0 e^{2\|q\|_{L^\infty}}, \end{aligned} \tag{27}$$

where $H_0 := 2C_p(\|\nabla \overline{g}\|_{L^2} + e^{|\beta\lambda|} + e^{|\beta\kappa|})$, C_p is a Poincaré constant and κ and λ are constants. Finally, the definition of H^1-norm and inequality (27) lead to

$$\|u\|_{H^1} \leq He^{2\|q\|_{L^\infty}}, \tag{28}$$

where $H = H_0(1 + C_p^2)^{1/2}$.

To prove inequality (26), we assume that u_1 and u_2 satisfy (12) with coefficients $A_1 = e^{q_1} = \eta_1$ and $A_2 = e^{q_2} = \eta_2$. Then, we subtract the term $\nabla \cdot (e^{q_1}\nabla u_2)$ and take the inner product with $u_2 - u_1$. We follow a strategy similar to the first part of the proof for the difference $u_2 - u_1$ to obtain

$$\begin{aligned} \|\nabla(u_2 - u_1)\|_{L^2} &\leq \|q_1 - q_2\|_{L^\infty} e^{4\max(\|q_1\|_\infty, \|q_2\|_\infty)}\big(\|\nabla \overline{g}\|_{L^2} + C_p e^{|\beta\lambda_2|} + C_p e^{|\beta\kappa_2|} + C_p|e^{\beta\max(\lambda_1,\lambda_2)} - e^{-\beta\max(\lambda_1,\lambda_2)}|\big) \\ &= S_0\|q_1 - q_2\|_{L^\infty} e^{4\max(\|q_1\|_\infty, \|q_2\|_\infty)}, \end{aligned}$$

where $S_0 := \|\nabla \overline{g}\|_{L^2} + C_p e^{|\beta\lambda_2|} + C_p e^{|\beta\kappa_2|} + C_p|e^{\beta\max(\lambda_1,\lambda_2)} - e^{-\beta\max(\lambda_1,\lambda_2)}|$, and $\kappa_i \leq u_i \leq \lambda_i$, $i \in \{1, 2\}$ are the pointwise estimates for the solution of the nonlinear Poisson–Boltzmann equation [43], where κ_i and λ_i are constants. Now, we can write

$$\begin{aligned} \|u_1 - u_2\|_{H^1} &\leq (1 + C_p^2)^{1/2}\|\nabla(u_1 - u_2)\|_{L^2} \\ &\leq (1 + C_p^2)^{1/2}\big(\|\nabla \overline{g}\|_{L^2} + C_p e^{|\beta\lambda_2|} + C_p e^{|\beta\kappa_2|} + C_p|e^{\beta\max(\lambda_1,\lambda_2)} - e^{-\beta\max(\lambda_1,\lambda_2)}|\big)\, e^{4\max(\|q_1\|_\infty, \|q_2\|_\infty)}\|q_1 - q_2\|_{L^\infty} \\ &= Se^{4\max(\|q_1\|_\infty, \|q_2\|_\infty)}\|q_1 - q_2\|_{L^\infty}, \end{aligned}$$

where $S := S_0(1 + C_p^2)^{1/2}$, which completes the proof. □

In [22], we solved the EIT inverse problem corresponding to the nonlinear model (12) on the cross-section of a right leg using real-world surface electrode measurements in order to identify the electrical conductivity of muscle tissue inside the leg. To this end, we developed a Bayesian inversion theory for the proposed EIT model and proposed an adaptive Markov-chain Monte-Carlo (MCMC) method in order to solve the EIT inverse problem.

One of the main challenges is the sensitivity of the conductivity on the boundary measurements, which results from the severely ill-posed and nonlinear EIT inverse problem. In this paper, we aim to deal with this challenge by optimizing the EIT experimental designs. More precisely, the goal is to determine the optimal frequency and

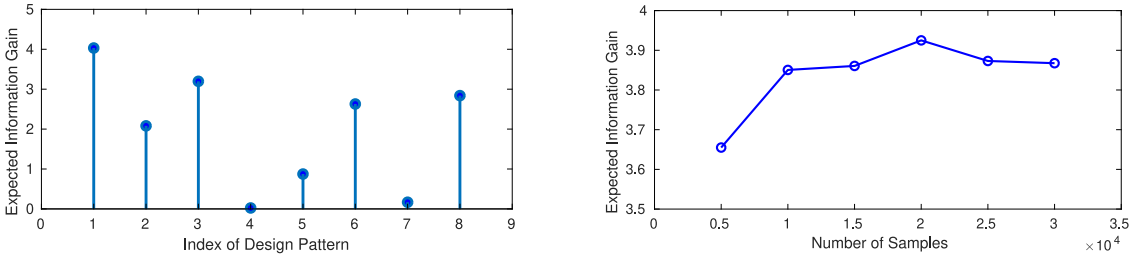

Fig. 3. The expected information gain for different design patterns used in Fig. 2 in order to extract the conductivity of the muscle as a parameter of interest in the frequency 50 kHz (left). The expected information gain for different numbers of samples used in Bayesian inversion process in the frequency 50 kHz (right).

electrode configuration in EIT based on the statistical interpretation of the reconstruction problem. The next section is dedicated to the optimal Bayesian experimental design for EIT by means of maximizing the expected information gain of the parameter extraction in Bayesian inference process, whose methodology was explained in Section 2.

4. Optimal Bayesian experimental design results

As mentioned, the sensitivity of the electrical properties such as conductivity on the boundary measurements due to the severely ill-posed and nonlinear EIT inverse problem leads to optimize the effective experimental designs in the problem in order to extract the unknown quantity as accurately as possible. Therefore, the goal here is to optimize Bayesian inversion applied to the EIT problem in order to find optimal Bayesian experimental designs including optimal frequency, optimal electrode placement, and optimal measurement strategies. In this section, we simulate the optimal Bayesian inversion methodology and illustrate the numerical results for the example of a cross-section of a right leg as a real-world application of EIT. The goal is to extract the electrical conductivity of muscle inside the right leg using the optimal Bayesian inversion mechanism. First, we present the results of calculated expected information gain for the posterior Markov-chain generated by the DRAM [47] as an adaptive MCMC reconstruction algorithm and using the nonlinear Poisson–Boltzmann equation as the EIT model.

In Fig. 3 (left), the calculated information gain corresponding to the 8 injection patterns used in Fig. 2 is illustrated. According to this result, the information that we can obtain from different EIT design patterns is not the same. Fig. 3 (right) displays the information gain for different numbers of samples used in Bayesian inversion process. According to this figure, there is no significant difference between the information gain from 10 k samples and more than 10 k in our EIT problem. That makes it possible to use the lower value 10 k as the number of samples in our calculations. This prior knowledge regarding an optimal number of samples will lead us to efficient and low-cost calculations without losing (much) information.

Algorithm 2 The optimal Bayesian inversion algorithm

Choose $\mathbf{d}_1 \in \mathcal{D}$ as the initial vector of the EIT design parameters.
for $k = 1 : N_{\text{iter}}$ **do**
1. Calculate the expected information gain for the design parameter $\mathbf{d}_k$ using the DLMC approximation Eq. (5).
2. Terminate the algorithm if the number of iterations has reached N_{iter}, express $\mathbf{d}_k$ as the optimal design.
3. Update $\mathbf{d}_k$ to a new value $\mathbf{d}_{k+1}$ using the recursive stochastic approximation form (see Section 2.3):

$$\mathbf{d}_{k+1} = \mathbf{d}_k - a_k \mathbf{g}_k(\mathbf{d}_k).$$

4. Replace $\mathbf{d}_k$ by $\mathbf{d}_{k+1}$.
end for

4.1. Optimal frequency for EIT measurements

In this section, numerical results of optimal Bayesian inversion for the estimation of optimal frequency for the EIT inverse problem, namely the extraction of the conductivity of a human leg muscle, are presented. Variation

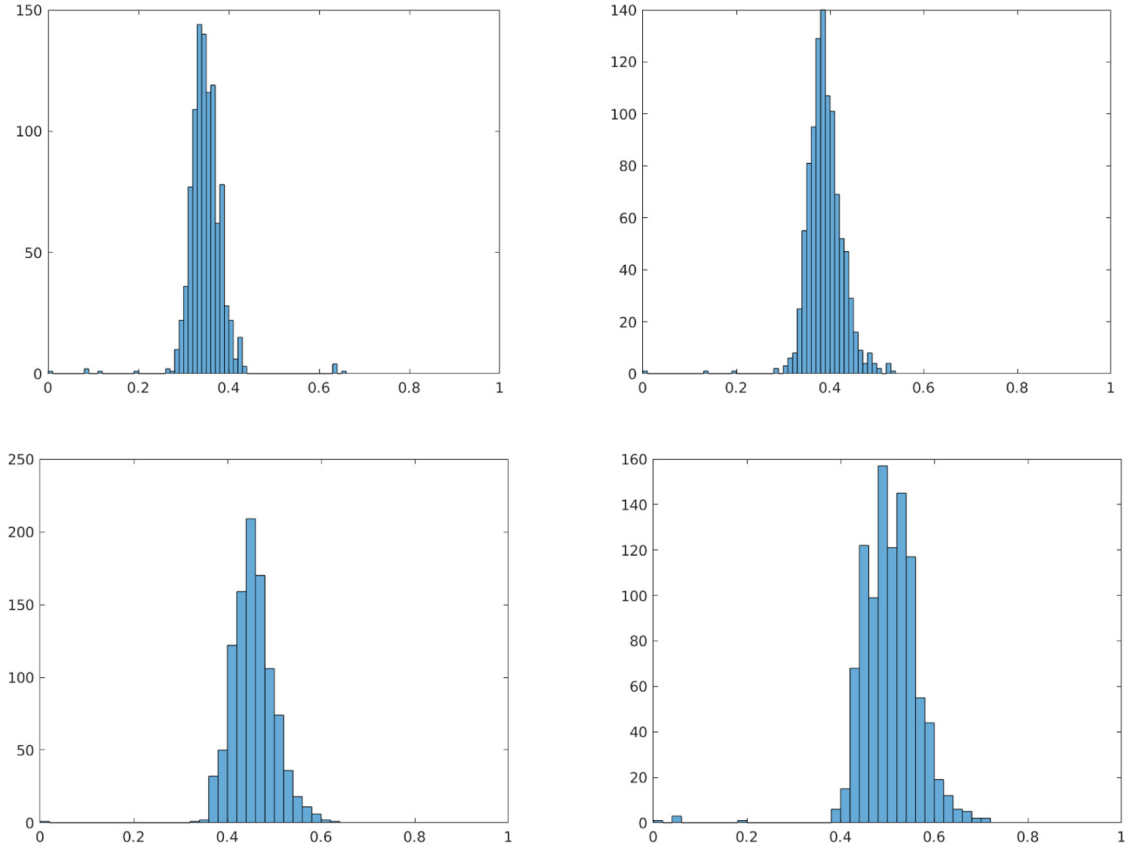

Fig. 4. Posterior distributions of the muscle conductivity for frequencies 10, 200, 500 and 900 kHz.

in the applied frequency as an EIT experimental design results in different Bayesian analysis. In Fig. 4, the posterior distribution of the generated Markov-chains for four different frequencies is illustrated. According to these results, the chains obtained for different frequencies have different characteristics and contain different amounts of information.

These results motivated us to calculate the expected information gain of each frequency in the range from 1 kHz to 1 MHz, which was very costly and time-consuming. The results are displayed in Fig. 5.

To overcome the problem of cost and complexity of calculations in order to reach a real-time experimental design in the EIT problem on one hand, and according to the noisy objective function (see Fig. 5) on the other hand, we employed a stochastic optimization method, namely the simultaneous perturbation stochastic approximation (SPSA), which was explained in Section 2. This method is applied to the problem of maximization of the expected information gain in order to obtain optimal and more informative experimental designs. According to the numerical results, the optimal frequency for the described EIT problem is estimated as 162 kHz. Table 1 includes the results for different frequencies.

In the optimal frequency, the conductivity of the muscle as the mean of posterior chain is estimated more accurately and the distribution of the posterior has the highest expected information gain compared to other non-optimal frequencies. Fig. 6 shows the posterior distribution and trajectory of the parameter of interest at the optimal frequency 162 kHz in our EIT problem.

4.2. Optimal electrode configuration for EIT measurements

Due to the nonlinearity and ill-posedness of the EIT inverse problem, any small variation in the electrode configuration leads to a big change in the gained information in Bayesian extraction process. In this section, we aim

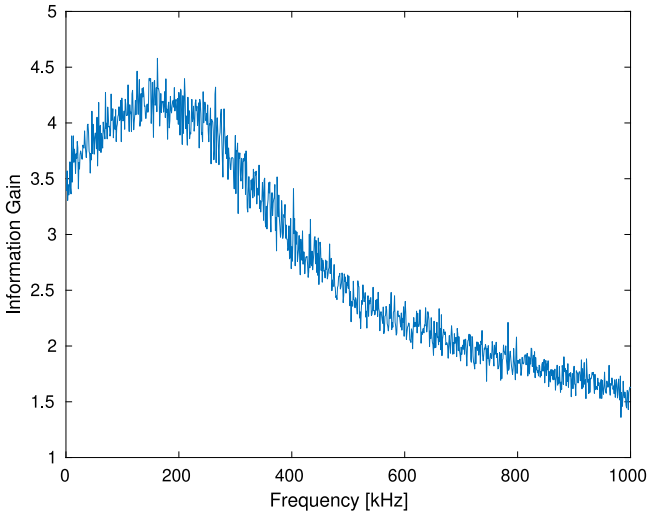

Fig. 5. The calculated expected information gains for different frequencies.

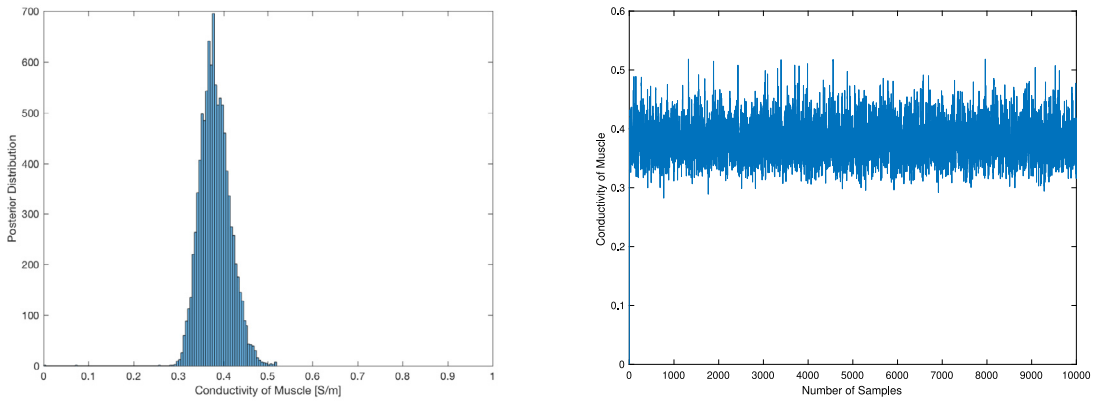

Fig. 6. The posterior distribution (left) and trace plot (right) of muscle conductivity for the obtained optimal frequency 162 kHz.

Table 1
Estimated mean values of muscle conductivity for various frequencies using Bayesian inference and corresponding calculated values of expected information gain.

Frequency kHz	Conductivity (True value)	Conductivity (Estimated)	Error of estimation	Expected information gain
10	0.3410	0.3500	0.0090	3.7819
162 (Optimal)	0.3754	0.3811	0.0057	4.4557
200	0.3840	0.3905	0.0065	4.1200
500	0.4460	0.4535	0.0075	2.4660
900	0.4950	0.5069	0.0119	1.7007

to find the optimal electrode configuration including the optimal placement of injection and measurement electrodes as well as the optimal measurement strategies using the optimal Bayesian inversion methodology that we proposed in Section 2 and Algorithm 2. In Fig. 7, various electrodes placement is displayed. The calculated information gain for the extraction of the muscle conductivity and mean of the estimated posterior chain for the unknown quantity in each case are indicated in the figures as well. The numerical experiments confirm the sensitivity of the EIT inverse problem on the electrode configuration and measurement strategy.

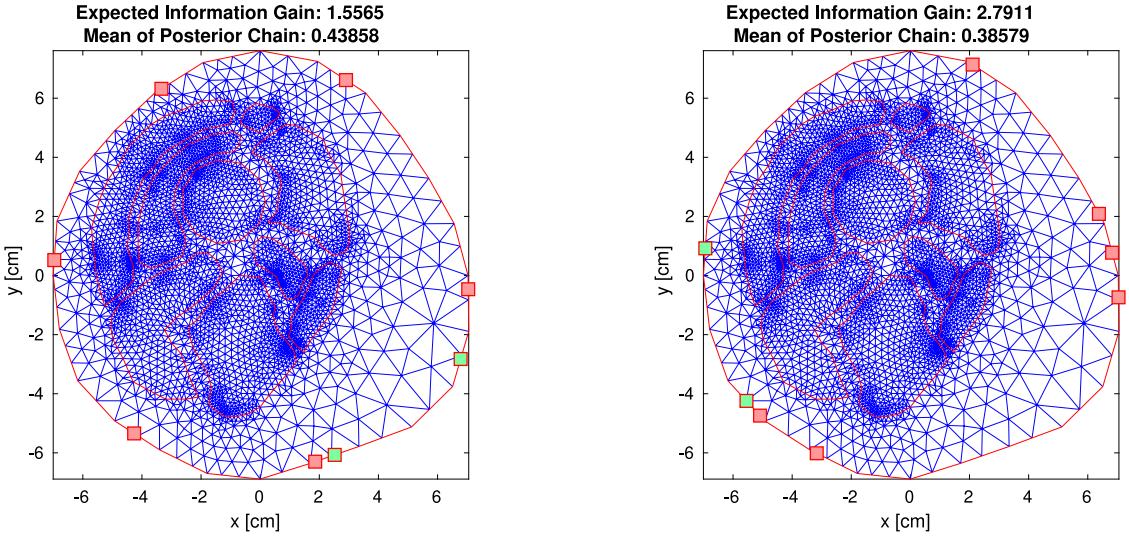

Fig. 7. Various electrode positioning together with the corresponding expected information gains and means of the estimated posterior chains are illustrated. Green electrodes are the injection pairs and red ones are measurement electrodes. (For interpretation of the references to color in this figure legend, the reader is referred to the web version of this article.)

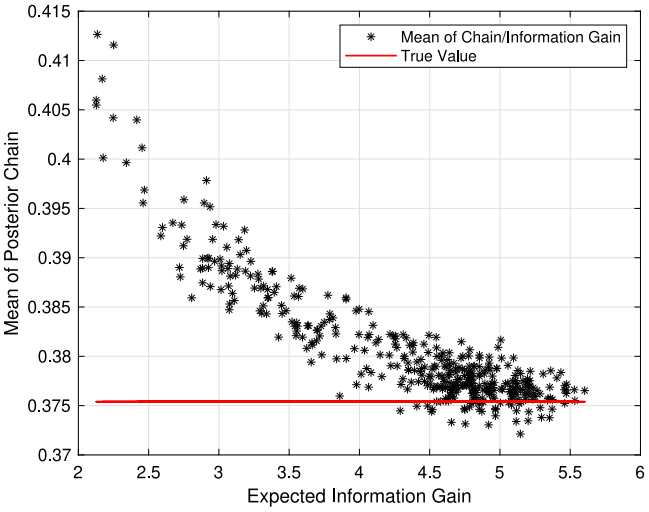

Fig. 8. Mean of the posterior chains in the optimization process versus the corresponding expected information gains.

Fig. 8 depicts the mean of the posterior chains generated in the optimization process versus the corresponding expected information gains. This figure illustrates the convergence of the means to the true value of the muscle conductivity, i.e., 0.3754, while reaching the maximum information gain using the optimal electrode configurations chosen by the optimization algorithm.

4.2.1. Clustering the electrode configurations

Since the objective function is noisy, it is hard to decide exactly which configuration is eventually the optimal one. According to various injection patterns, we need to use two and even more (near) optimal electrode configurations for the process of the measurement and image reconstruction. Therefore, we split the obtained configurations into the optimal and non-optimal ones and to this end we apply data clustering methods. The K-means algorithm is one of the most preferred clustering tools in data mining for many real world applications [48,49]. Although this clustering method is simple to understand and deploy, it suffers from some limitations; due to the use of the Euclidean distance,

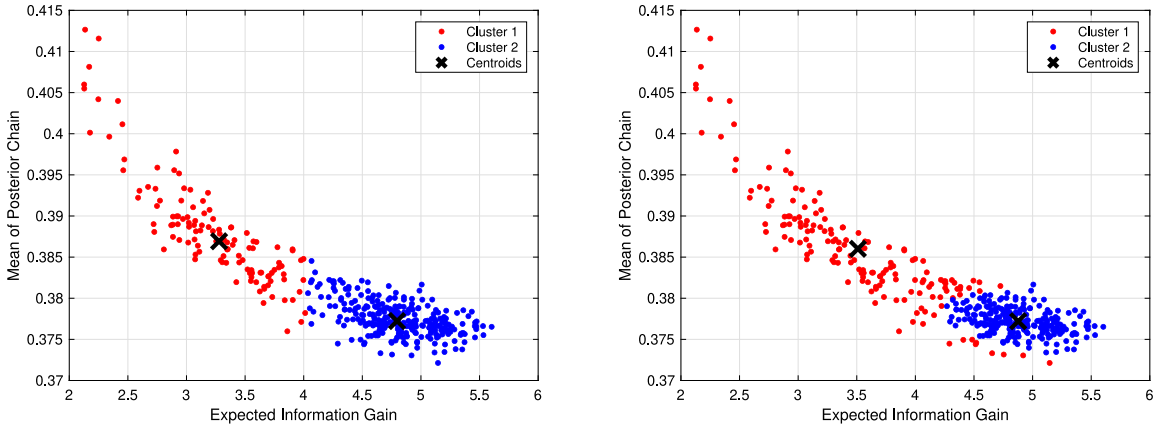

Fig. 9. Optimal (blue) and non-optimal (red) electrode configuration clusters using K-means clustering method (left) and MAP-DP method (right). (For interpretation of the references to color in this figure legend, the reader is referred to the web version of this article.)

K-means assumes that the data space is isotropic in the sense that distances are unchanged by translations and rotations and therefore each cluster consists of the data points lying within a sphere around the centroid. One of the limitations of K-means is that this method implicitly assumes all clusters have the same radius while sometimes they are very clearly identifiable. Additionally, K-means implicitly assumes each cluster has the same volume in data space in the sense that each cluster contains the same number of data points, while there might be significant differences in clusters density. Another limitation is that small changes in the data result in small changes to the position of the cluster centroid, which is assumed as average of the data points in a cluster. Therefore, outliers can significantly impair the results of K-means. Moreover, in the method of K-means it is assumed that the number K of clusters is given, while this is rarely the case in practice. These limitations lead to inaccurate conclusions about the structure in the data.

To overcome these limitations, we apply maximum a-posteriori Dirichlet process mixtures (MAP-DP) algorithm [50]. This method is statistically rigorous and it is based on nonparametric Bayesian Dirichlet process mixture modeling, which is a probabilistic model and involves fitting a probability density model to the data, while K-means is essentially geometric. This method for instance estimates the number of necessary clusters for given data points using Bayesian nonparametric (BNP) models [51] as well as it separates outliers from the data efficiently and thus the centroid is estimated accurately. Fig. 9 demonstrates the optimal and non-optimal electrode configuration clusters using the two methods, i.e., K-means and MAP-DP algorithms. This figure clearly illustrates the efficiency of the MAP-DP compared to the K-means by more accurately identifying the optimal configurations.

In Fig. 10, the standard uniform electrode configuration versus two optimal design patterns with high expected information gains is displayed. The optimal patterns are proposed by the applied optimization method on Bayesian results of the EIT inverse problem and they belong to the optimal cluster. Due to these results, injection from the top-left of the computational domain with measurement electrodes which are close together leads to a larger information gain and more accurate estimation of the muscle conductivity, whose true value is 0.3754, while uniformly distributed electrodes result in a moderate information gain and an inaccurate estimation of the unknown quantity compared to the optimal configurations. All experiments are performed in the optimal frequency of 162 kHz, which was calculated in Section 4.1.

The results of various electrode configurations shown in Figs. 7 and 10 including the corresponding expected information gain and the estimated value for the muscle conductivity using Bayesian inversion are summarized in Table 2. The comparison shows the efficiency of the presented optimal Bayesian inversion for the EIT inverse problem.

5. Conclusions

We developed an optimal algorithm for Bayesian inversion for the EIT problem, which has applications in medical imaging. The new inversion methodology presents an optimal EIT experimental design recipe including

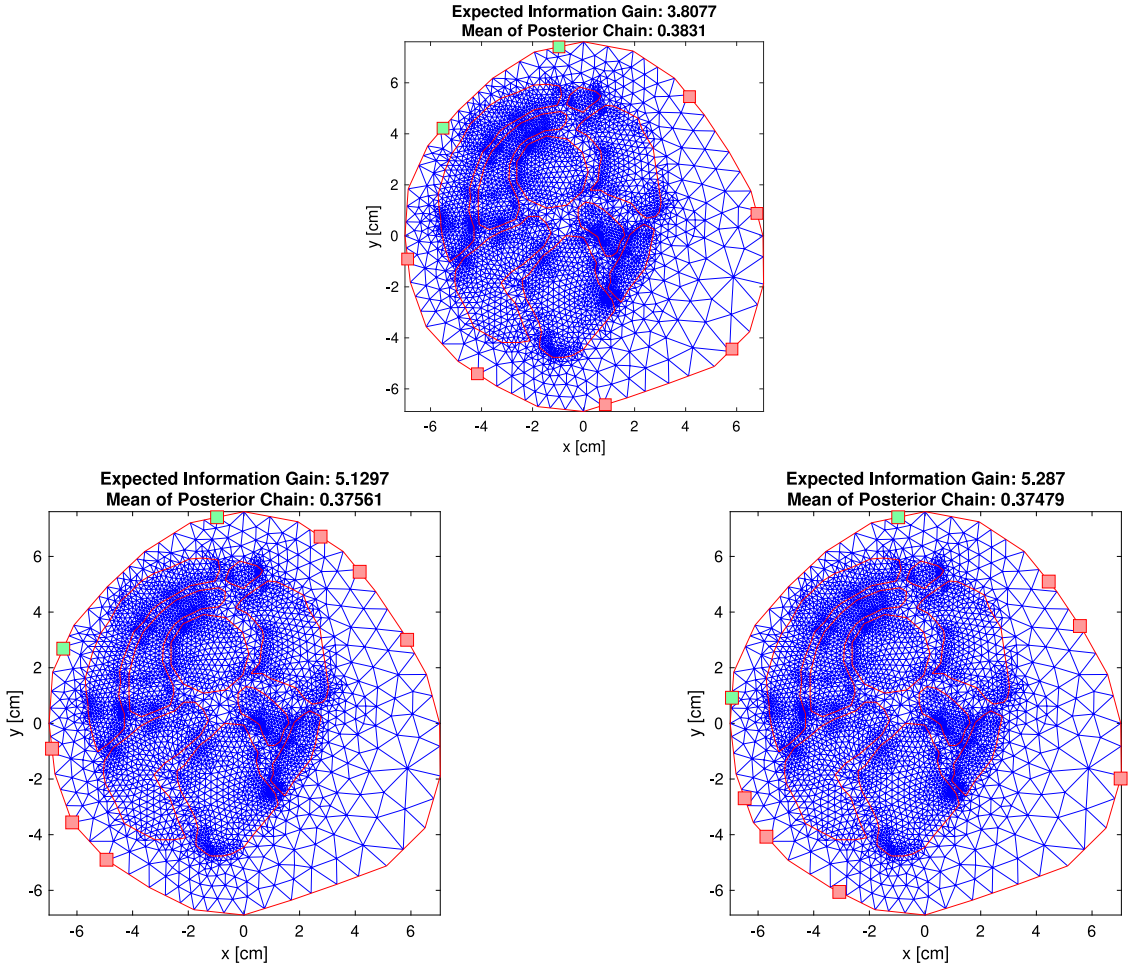

Fig. 10. Standard uniform (top) electrode configuration versus optimal (bottom) configurations with the highest expected information gains and estimations of the muscle conductivity closest to its true value.

Table 2
Estimated expected information gains and mean of Markov chains for the muscle conductivity (true value: 0.3754) for various electrode configurations.

Electrode configuration	Expected information gain	Estimated muscle conductivity
Non-optimal I (Fig. 7-left)	1.5565	0.4386
Non-optimal II (Fig. 7-right)	2.7911	0.3858
Uniform (Fig. 10-top)	3.8077	0.3831
Optimal I (Fig. 10-bottom left)	5.1297	0.3756
Optimal II (Fig. 10-bottom right)	5.2870	0.3748

the optimal frequency and electrode configuration by maximizing the expected information gain in the inversion process, which results in accurate estimation of EIT model unknowns and high-resolution medical images. To this end, we developed a double-loop Monte-Carlo method and simultaneous perturbation stochastic approximation for the EIT inverse problem. The comparison of numerical results for various electrode configurations indicates the efficiency of the proposed optimal Bayesian inversion methodology for the EIT problem. It is valuable to mention that the optimal sensor placement would be affected by the object to be imaged and updates to the configuration would be needed as the object is imaged. In clinical practice, electrode configurations should be implemented by more advanced EIT devices.

Declaration of competing interest

The authors declare that they have no known competing financial interests or personal relationships that could have appeared to influence the work reported in this paper.

Acknowledgment

The authors acknowledge support by FWF (Austrian Science Fund) START Project No. Y660 *PDE Models for Nanotechnology*.

References

[1] L. Taghizadeh, A. Karimi, E. Presterl, C. Heitzinger, Bayesian inversion for a biofilm model including quorum sensing, Comput. Biol. Med. 117 (2020) 103582.
[2] E.K. Lenzi, L.R. Evangelista, L. Taghizadeh, D. Pasterk, R.S. Zola, T. Sandev, C. Heitzinger, I. Petreska, Reliability of Poisson–Nernst–Planck anomalous models for impedance spectroscopy, J. Phys. Chem. B 123 (37) (2019) 7885–7892.
[3] B. Stadlbauer, A. Cossettini, D. Pasterk, P. Scarbolo, L. Taghizadeh, C. Heitzinger, L. Selmi, Bayesian estimation of physical and geometrical parameters for nanocapacitor array biosensors, J. Comput. Phys. 397 (2019) 108874.
[4] J.G. Webster, Electrical Impedance Tomography, Taylor & Francis Group, 1990.
[5] C.W.L. Denyer, Electronics for Real-Time and Three-Dimensional Electrical Impedance Tomographs (Ph.D. thesis), Oxford Brookes University, 1996.
[6] M. Cheney, D. Isaacson, J.C. Newell, Electrical impedance tomography, SIAM Rev. 41 (1) (1999) 85–101.
[7] L. Borcea, Electrical impedance tomography, Inverse Problems 18 (6) (2002) R99.
[8] D.S. Holder, Electrical Impedance Tomography: Methods, History and Applications, CRC Press, 2004.
[9] I. Frerichs, J. Hinz, P. Herrmann, G. Weisser, G. Hahn, T. Dudykevych, M. Quintel, G. Hellige, Detection of local lung air content by electrical impedance tomography compared with electron beam CT, J. Appl. Physiol. 93 (2) (2002) 660–666.
[10] T. Meier, H. Luepschen, J. Karsten, T. Leibecke, M. Großherr, H. Gehring, S. Leonhardt, Assessment of regional lung recruitment and derecruitment during a PEEP trial based on electrical impedance tomography, Intensive Care Med. 34 (3) (2008) 543–550.
[11] N. Harris, A. Suggett, D. Barber, B. Brown, Applications of applied potential tomography (APT) in respiratory medicine, Clin. Phys. Physiol. Meas. 8 (4A) (1987) 155.
[12] A. Adler, Y. Berthiaume, R. Guardo, R. Amyot, Imaging of pulmonary edema with electrical impedance tomography, in: Proceedings of 17th International Conference of the Engineering in Medicine and Biology Society, Vol. 1, IEEE, 1995, pp. 557–558.
[13] R.J. Halter, A. Hartov, K.D. Paulsen, A broadband high-frequency electrical impedance tomography system for breast imaging, IEEE Trans. Biomed. Eng. 55 (2) (2008) 650–659.
[14] V. Cherepenin, A. Karpov, A. Korjenevsky, V. Kornienko, A. Mazaletskaya, D. Mazourov, D. Meister, A 3D electrical impedance tomography (EIT) system for breast cancer detection, Physiol. Meas. 22 (1) (2001) 9.
[15] D. Holder, A. Rao, Y. Hanquan, Imaging of physiologically evoked responses by electrical impedance tomography with cortical electrodes in the anaesthetized rabbit, Physiol. Meas. 17 (4A) (1996) A179.
[16] D. Holder, Electrical impedance tomography (EIT) of brain function, Brain Topogr. 5 (2) (1992) 87–93.
[17] T. Tidswell, A. Gibson, R.H. Bayford, D.S. Holder, Three-dimensional electrical impedance tomography of human brain activity, Neuroimage 13 (2) (2001) 283–294.
[18] W.R. Lionheart, EIT reconstruction algorithms: pitfalls, challenges and recent developments, Physiol. Meas. 25 (1) (2004) 125.
[19] A. Sinton, B. Brown, D. Barber, F. McArdle, A. Leathard, Noise and spatial resolution of a real-time electrical impedance tomograph, Clin. Phys. Physiol. Meas. 13 (A) (1992) 125.
[20] J.L. Wheeler, W. Wang, M. Tang, A comparison of methods for measurement of spatial resolution in two-dimensional circular EIT images, Physiol. Meas. 23 (1) (2002) 169.
[21] A. Adler, R. Guardo, A neural network image reconstruction technique for electrical impedance tomography, IEEE Trans. Med. Imaging 13 (4) (1994) 594–600.
[22] L. Taghizadeh, A. Karimi, B. Stadlbauer, W.J. Weninger, E. Kaniusas, C. Heitzinger, Bayesian inversion for electrical-impedance tomography in medical imaging using the nonlinear Poisson–Boltzmann equation, Comput. Methods Appl. Mech. Engrg. 365 (2020) 112959.
[23] R.C. Smith, Uncertainty Quantification: Theory, Implementation, and Applications, Vol. 12, SIAM, 2013.
[24] A. Gelman, J.B. Carlin, H.S. Stern, D.B. Dunson, A. Vehtari, D.B. Rubin, Bayesian Data Analysis, Chapman and Hall/CRC, 2013.
[25] J. Kaipio, E. Somersalo, Statistical and Computational Inverse Problems, Springer Science & Business Media, 2006.
[26] A. Tarantola, Inverse Problem Theory and Methods for Model Parameter Estimation, SIAM, 2005.
[27] J. Kaipio, A. Seppänen, E. Somersalo, H. Haario, Posterior covariance related optimal current patterns in electrical impedance tomography, Inverse Problems 20 (3) (2004) 919.
[28] P. Tsilifis, R.G. Ghanem, P. Hajali, Efficient Bayesian experimentation using an expected information gain lower bound, SIAM/ASA J. Uncertain. Quantif. 5 (1) (2017) 30–62.
[29] Q. Long, M. Scavino, R. Tempone, S. Wang, Fast estimation of expected information gains for Bayesian experimental designs based on Laplace approximations, Comput. Methods Appl. Mech. Engrg. 259 (2013) 24–39.

[30] D. Smyl, D. Liu, Optimizing electrode positions in 2D electrical impedance tomography using deep learning, IEEE Trans. Instrum. Meas. (2020).
[31] N. Hyvonen, A. Seppänen, S. Staboulis, Optimizing electrode positions in electrical impedance tomography, SIAM J. Appl. Math. 74 (6) (2014) 1831–1851.
[32] D.V. Lindley, et al., On a measure of the information provided by an experiment, Ann. Math. Stat. 27 (4) (1956) 986–1005.
[33] C.E. Shannon, A mathematical theory of communication, Bell Syst. Tech. J. 27 (3) (1948) 379–423.
[34] S. Kullback, Information Theory and Statistics, Courier Corporation, 1997.
[35] S. Kullback, R.A. Leibler, On information and sufficiency, Ann. Math. Stat. 22 (1) (1951) 79–86.
[36] J.C. Spall, Introduction to Stochastic Search and Optimization: Estimation, Simulation, and Control, Vol. 65, John Wiley & Sons, 2005.
[37] J.C. Spall, et al., Multivariate stochastic approximation using a simultaneous perturbation gradient approximation, IEEE Trans. Automat. Control 37 (3) (1992) 332–341.
[38] X. Huan, Y. Marzouk, Gradient-based stochastic optimization methods in Bayesian experimental design, Int. J. Uncertain. Quantif. 4 (6) (2014).
[39] X. Huan, Y.M. Marzouk, Simulation-based optimal Bayesian experimental design for nonlinear systems, J. Comput. Phys. 232 (1) (2013) 288–317.
[40] J.C. Spall, An overview of the simultaneous perturbation method for efficient optimization, Johns Hopkins APL Tech. Dig. 19 (4) (1998) 482–492.
[41] J.C. Spall, Implementation of the simultaneous perturbation algorithm for stochastic optimization, IEEE Trans. Aerosp. Electron. Syst. 34 (3) (1998) 817–823.
[42] A. Adler, W.R. Lionheart, Uses and abuses of EIDORS: an extensible software base for EIT, Physiol. Meas. 27 (5) (2006) S25.
[43] S. Baumgartner, C. Heitzinger, Existence and local uniqueness for 3D self-consistent multiscale models for field-effect sensors, Commun. Math. Sci. 10 (2) (2012) 693–716.
[44] C. Schwab, A.M. Stuart, Sparse deterministic approximation of Bayesian inverse problems, Inverse Problems 28 (4) (2012) 045003.
[45] V.H. Hoang, C. Schwab, A.M. Stuart, Complexity analysis of accelerated MCMC methods for Bayesian inversion, Inverse Problems 29 (8) (2013) 085010.
[46] A.M. Stuart, Inverse problems: a Bayesian perspective, Acta Numer. 19 (2010) 451–559.
[47] H. Haario, M. Laine, A. Mira, E. Saksman, DRAM: efficient adaptive MCMC, Stat. Comput. 16 (4) (2006) 339–354.
[48] P. Berkhin, A survey of clustering data mining techniques, in: Grouping Multidimensional Data: Recent Advances in Clustering, Springer Science & Business Media, 2006, pp. 25–71.
[49] S. Lloyd, Least squares quantization in PCM, IEEE Trans. Inform. Theory 28 (2) (1982) 129–137.
[50] Y.P. Raykov, A. Boukouvalas, F. Baig, M.A. Little, What to do when K-means clustering fails: a simple yet principled alternative algorithm, PLoS One 11 (9) (2016) 1–28.
[51] N.L. Hjort, C. Holmes, P. Müller, S.G. Walker, Bayesian Nonparametrics, Vol. 28, Cambridge University Press, 2010.